Theoretical and Experimental Verification of Independent Control for Parallel-Connected Multi-UPS's

Eduardo Kazuhide Sato†, Atsuo Kawamura†, and Ryo Fujii‡

Department of Electrical and Computer Engineering
Yokohama National University†
79-5, Tokiwadai, Hodogaya-ku, Yokohama, 240-8501 Japan
{kawamura, eduardo}@kawalab.dnj.ynu.ac.jp

Hitachi Industrial Equipment Systems Co., Ltd.‡
1-2-1, Kinrakuji-cho, Amagasaki, Hyogo, 660-0806 Japan

Abstract:

This paper proposes an independent control for parallel-connected multi UPS's made of two simple PI controllers for the active and reactive components currents. The phase and the amplitude of the voltage source are the controllable variables here. The current is measured locally and, with the computation of the active and reactive components, the control ensure the synchronization and load sharing. Theoretical analysis and experimental results confirm the efficiency of the control.

1.0 Introduction

Critical loads such as computer systems and communications plants play a significant role in our daily lives so that standards and regulations recommend to them a continuous supply of electrical energy even in a worst-case scenario as in power utility outage. To attend this precept, the uninterruptible power supply (UPS) is employed as a backup emergency power source acting as a local power supply system replacing a failed conventional utility network.

Depending on the necessity, a parallel-connection of multi UPS's enables large capacity and higher reliability UPS systems. However some providences should be taken in order to guarantee the feasibility of the operation [1]. One important item is regarding to the control scheme for parallel operation.

When multiple UPS's are connected in parallel, usually the output current information is collected to a master UPS which directs the commands to others UPS's. As a result, the load sharing is achieved and, at the same time, the lateral reactive current is also controlled. Although it has a certain efficacy, a remaining defficiency of this control method is the lack of true redundancy because of the dependency of the master.

The independent control for parallel-connected multi-UPS was proposed in [3], in which the multiple UPS's are connected in parallel without the exchange of any information, and still they can automatically achieve the load sharing and the synchronization. However, the theoretical proof for the stable operation was not succeeded before. Thus, in this paper the theoretical analysis and the proof of the stability is shown and the experimental verification is presented.

2.0 System Modeling and Analysis

2.1 System Modeling and Control

Fig. 1 depicts an elementary parallel-connected UPS system with an attached load where the voltage v of each UPS (unit) is expressed by (1)

$$v = (V_M + dv)\cos(\omega t + hs) \tag{1}$$

where V_M is the voltage amplitude; ω is the angular frequency; and hs and dv are the controllable variables.

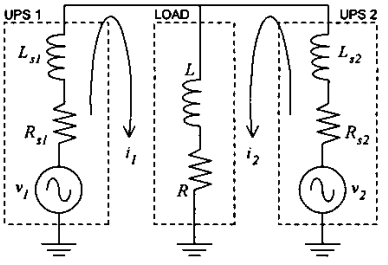

Fig. 1: An elementary parallel-connected UPS system with two units connected to a common point of contact and feeding a certain load

The phase angle hs and amplitude dv of the voltage v are controlled by a simple proportional-integral (PI) control scheme defined by (2) and (3)

$$hs = kp_1(I_{pref} - I_p) + kp_2 \int_0^t (I_{pref} - I_p)dt \tag{2}$$

$$dv = kq_1(I_{qref} - I_q) + kq_2 \int_0^t (I_{qref} - I_q)dt \tag{3}$$

where kp_1, kp_2, kq_1 and kq_2 are gains; and I_p and I_q represent the active and reactive current, respectively.

Initially, the current in each unit is measured locally and its active and reactive components are calculated by (4) and (5)

$$I_p = \frac{2}{T}\int_{t-T}^{t} i(t)\cos(\omega t + hs)dt \tag{4}$$

$$I_q = \frac{2}{T}\int_{t-T}^{t} i(t)\sin(\omega t + hs)dt \tag{5}$$

where i is the output current in each unit; and T is the inverse of the frequency.

This computation leads to some ripples during the transient, thus, the process uses a low pass filter (6) (7)

$$I_{pout} = a\int_0^t (I_p - I_{pout})dt \tag{6}$$

$$I_{qout} = a\int_0^t (I_q - I_{qout})dt \tag{7}$$

where a is the filter constant.

(4), (5), (6) and (7) constitute the algorithm to calculate the current components [3].

2.2 *Explanation*

One explanation for the independent control considers the synchronous machine model and its swing equation (8) [4]

$$J\frac{d}{dt}\omega = T_m - (T_e + B\omega) \tag{8}$$

where T_m is the mechanical turbine torque; T_e is the electromagnetic torque; J is the moment of inertia of the mechanical model; B is the damping torque coefficient; and ω is the rotor angular velocity.

When $T_m \neq T_e$, an angular velocity deviation $\Delta\omega$ is taken into account and (8) becomes

$$J\frac{d}{dt}\Delta\omega = T_m - (T_e + B\Delta\omega). \tag{9}$$

Multiplying (9) to ω_0 and considering $P = T\omega_0 = VI$, the swing equation in terms of $\Delta\omega$ becomes

$$\frac{d}{dt}\Delta\omega = \frac{V}{J\omega_0}(I_{pref} - I_p) - \frac{B}{J}\Delta\omega \tag{10}$$

Solving the differential equation (10) for $t \to \infty$ yields

$$\Delta\omega(t \to \infty) = \frac{V}{B\omega_0}(I_{pref} - I_p) \tag{11}$$

Since

$$hs = \int \Delta\omega dt, \tag{12}$$

the constant $V/B\omega_0$ in (11) is considered the gain kp_2 in (2). Thus,

$$hs = \int_0^t\int_0^t \left[\alpha_1(I_{pref} - I_p) - \beta_1\Delta\omega\right]dtdt \tag{13}$$

where

$$\alpha_1 = \frac{V}{J\omega_0} = \frac{kp_2}{\tau} \tag{14}$$

$$\beta_1 = \frac{B}{J} = \frac{1}{\tau}, \tag{15}$$

and τ is defined as a time constant.

If (13) is the control equation for parallel-connected multi UPS's system, it will result in an unstable response [4] [5]. To solve this, a derivative term for the frequency is added to achieve the stability. Therefore (13) becomes

$$hs = kp_1(I_{pref} - I_p) + \int_0^t\int_0^t \left[\alpha_1(I_{pref} - I_p) - \beta_1\Delta\omega\right]dtdt. \tag{16}$$

where kp_1 is considered the same as in (2).

2.3 *Analysis of the System and Control*

This analysis has a methodology as similar as in [6] although the control equations are different. Considering (17) as an extension of (16) for dv

$$dv = kq_1(I_{qref} - I_q) + \int_0^t\int_0^t [\alpha_2(I_{qref} - I_q) - \beta_2\dot{dv}]dtdt \tag{17}$$

where, for this analysis,

$$\alpha_2 = \frac{kq_2}{\tau} \text{ and } \beta_2 = \frac{1}{\tau}.$$

The linear representation of (16) and (17) in frequency domain is

$$s^2\Delta hs(s) = -kp_1\Delta\ddot{I}_p - \alpha_1\Delta I_p(s) - \beta_1 s\Delta hs(s) \tag{18}$$

$$s^2\Delta dv(s) = -kq_1\Delta\ddot{I}_q - \alpha_2\Delta I_q(s) - \beta_2 s\Delta dv(s) \tag{19}$$

where s is the Laplace operator and Δ indicates the deviation of the variable around the equilibrium point.

Considering the low pass filter used in the calculation of the current components, equations (6) and (7) are, in frequency domain,

$$I_{pout}(s) = \frac{a}{s+a}I_p(s) \tag{20}$$

$$I_{qout}(s) = \frac{a}{s+a}I_q(s). \tag{21}$$

I_p in (18) and I_q in (19) are actually I_{pout} in (20) and I_{qout} in (21), respectively, so that the linearized control equations are, in the time domain,

$$\Delta\ddot{hs} = -(a+\beta_1)\Delta\ddot{hs} - a\beta_1\Delta\dot{hs} - a\alpha_1\Delta I_p - akp_1\Delta\ddot{I}_p \tag{22}$$

$$\Delta\ddot{dv} = -(a+\beta_2)\Delta\ddot{dv} - a\beta_2\Delta\dot{dv} - a\alpha_2\Delta I_q - akq_1\Delta\ddot{I}_q. \tag{23}$$

Considering the rotating coordinates as in Fig. 2, the vector $\vec{V}$ and angle hs are expressed as in (24) and (25)

$$V = |\vec{V}| = \sqrt{v_d^2 + v_q^2} \tag{24}$$

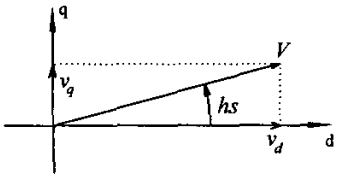

Fig. 2: d-q rotating coordinates supporting a vector $\vec{V}$ displaced by an angle hs

$$hs = \arctan\left(\frac{v_q}{v_d}\right) \tag{25}$$

Linearizing (24) and (25) yields

$$\Delta hs = r_d \Delta v_d + r_q \Delta v_q \tag{26}$$

$$\Delta V = s_d \Delta v_d + s_q \Delta v_q \tag{27}$$

where

$$\begin{cases} r_d = -\dfrac{v_q}{v_d^2 + v_q^2} \\ r_q = \dfrac{v_d}{v_d^2 + v_q^2} \end{cases} \qquad \begin{cases} s_d = \dfrac{v_d}{\sqrt{v_d^2 + v_q^2}} \\ s_q = \dfrac{v_q}{\sqrt{v_d^2 + v_q^2}}. \end{cases}$$

Considering that $\Delta V = \Delta dv$ and solving the system formed by (22), (23), (26) and (27) for variables $\Delta\ddot{v}_d$ and $\Delta\ddot{v}_q$, we have

$$\begin{aligned} \Delta\ddot{v}_d = {} & \frac{(a+\beta_2)r_q s_d - (a+\beta_1)r_d s_q}{r_d s_q - r_q s_d}\Delta\ddot{v}_d + \\ & + \frac{(\beta_2 - \beta_1)r_q s_q}{r_d s_q - r_q s_d}\Delta\ddot{v}_q + \\ & + \frac{a(\beta_2 r_q s_d - \beta_1 r_d s_q)}{r_d s_q - r_q s_d}\Delta\dot{v}_d + \frac{a r_q s_q (\beta_2 - \beta_1)}{r_d s_q - r_q s_d}\Delta\dot{v}_q - \\ & - \frac{a\alpha_1 s_q}{r_d s_q - r_q s_d}\Delta I_p + \frac{a\alpha_2 r_q}{r_d s_q - r_q s_d}\Delta I_q - \\ & - \frac{akp_1 s_q}{r_d s_q - r_q s_d}\Delta\ddot{I}_p + \frac{akq_1 r_q}{r_d s_q - r_q s_d}\Delta\ddot{I}_q \end{aligned} \tag{28}$$

$$\begin{aligned} \Delta\ddot{v}_q = {} & \frac{(\beta_2 - \beta_1)r_d s_d}{r_q s_d - r_d s_q}\Delta\ddot{v}_d + \\ & + \frac{(a+\beta_2)r_d s_q - (a+\beta_1)r_q s_d}{r_q s_d - r_d s_q}\Delta\ddot{v}_q + \\ & + \frac{a r_d s_d (\beta_2 - \beta_1)}{r_q s_d - r_d s_q}\Delta\dot{v}_d + \frac{a(\beta_2 r_d s_q - \beta_1 r_q s_d)}{r_q s_d - r_d s_q}\Delta\dot{v}_q - \\ & - \frac{a\alpha_1 s_d}{r_q s_d - r_d s_q}\Delta I_p + \frac{a\alpha_2 r_d}{r_q s_d - r_d s_q}\Delta I_q \\ & - \frac{akp_1 s_d}{r_q s_d - r_d s_q}\Delta\ddot{I}_p + \frac{akq_1 r_d}{r_q s_d - r_d s_q}\Delta\ddot{I}_q. \end{aligned} \tag{29}$$

(22), (28) and (29) form a state equation which in matrix form is

$$\begin{bmatrix} \Delta\dddot{hs} \\ \Delta\ddot{v}_d \\ \Delta\ddot{v}_q \end{bmatrix} = \mathbf{M}\begin{bmatrix} \Delta\ddot{hs} \\ \Delta\dot{v}_d \\ \Delta\dot{v}_q \end{bmatrix} + \mathbf{G}\begin{bmatrix} \Delta\dot{hs} \\ \Delta v_d \\ \Delta v_q \end{bmatrix} + \mathbf{H}\begin{bmatrix} \Delta I_p \\ \Delta I_q \end{bmatrix}. \tag{30}$$

Considering the circuit as in Fig. 1, the currents I_1 and I_2 represent a pair of complex equations in terms of admittance and voltage (31)

$$\begin{bmatrix} \Delta I_1 \\ \Delta I_2 \end{bmatrix} = \begin{bmatrix} Y_{11} & Y_{12} \\ Y_{12} & Y_{22} \end{bmatrix}\begin{bmatrix} \Delta V_1 \\ \Delta V_2 \end{bmatrix} \tag{31}$$

which can be transformed into four real equations (32)

$$\begin{bmatrix} \Delta i_{d1} \\ \Delta i_{q1} \\ \Delta i_{d2} \\ \Delta i_{q2} \end{bmatrix} = \begin{bmatrix} G_{11} & -B_{11} & G_{12} & -B_{12} \\ B_{11} & G_{11} & B_{12} & G_{12} \\ G_{21} & -B_{21} & G_{22} & -B_{22} \\ B_{21} & G_{21} & B_{22} & G_{22} \end{bmatrix}\begin{bmatrix} \Delta v_{d1} \\ \Delta v_{q1} \\ \Delta v_{d2} \\ \Delta v_{q2} \end{bmatrix} \tag{32}$$

where $Y_{11} = G_{11} + jB_{11}$; $Y_{22} = G_{22} + jB_{22}$; $Y_{12} = G_{12} + jB_{12}$; and $Y_{21} = G_{21} + jB_{21}$.

By using a simple transformation, i_d and i_q can be converted to I_p and I_q [7] and (30) becomes

$$\begin{bmatrix} \Delta\dddot{hs} \\ \Delta\ddot{v}_d \\ \Delta\ddot{v}_q \end{bmatrix} = \mathbf{A_1}\begin{bmatrix} \Delta\ddot{hs} \\ \Delta\dot{v}_d \\ \Delta\dot{v}_q \end{bmatrix} + \mathbf{A_2}\begin{bmatrix} \Delta\dot{hs} \\ \Delta v_d \\ \Delta v_q \end{bmatrix} + \mathbf{A_3}\begin{bmatrix} \Delta hs \\ \Delta v_d \\ \Delta v_q \end{bmatrix}. \tag{33}$$

Equation (33) is the state equation of the system which can be transformed into a first order differential equation by means of (34)

$$\begin{bmatrix} \dot{y}_1 \\ \dot{y}_2 \\ \dot{y}_3 \end{bmatrix} = \begin{bmatrix} \mathbf{0} & \mathbf{1} & \mathbf{0} \\ \mathbf{0} & \mathbf{0} & \mathbf{1} \\ \mathbf{A_3} & \mathbf{A_2} & \mathbf{A_1} \end{bmatrix}\begin{bmatrix} y_1 \\ y_2 \\ y_3 \end{bmatrix} = \mathbf{A}\begin{bmatrix} y_1 \\ y_2 \\ y_3 \end{bmatrix}. \tag{34}$$

In case of two units, $\mathbf{A}$ is a 18×18 matrix. The analysis of the eigenvalues of $\mathbf{A}$ gives information about the dynamic performance of the system.

2.4. *Computation of the Eigenvalues of the Matrix A*

Considering the parameters given in the Table 1 and selecting some values for the gains of the control equations, several computations of eigenvalues can be obtained. The load resistance is taken to be 50 [Ω] and the load inductance is taken to be 100 [mH]. The voltage of both units is $80\sqrt{2}$ [V] ($v_d = 80\sqrt{2}$; $v_q = 0$) and the frequency is 50 Hz.

Table 1: Parameters for computation of the eigenvalues

	UPS 1		UPS 2
R_{s1}	0.5 Ω	R_{s2}	1 Ω
L_{s1}	1 mH	L_{s2}	2 mH
β_1, β_2	1	β_1, β_2	1
α_1	0.05	α_1	0.1
α_2	0	α_2	0
a	0.63	a	0.63
kp_1	0.5	kp_1	1.0
kq_1	0.5	kq_1	1.0

Table 2: Eigenvalues of matrix **A** for selected values of τ

	$\tau = 0.001$	$\tau = 1$	$\tau = 1000$
λ_1	- 0.30 + j1.7	- 0.0074 + j0.31	+ j0.0099
λ_2	- 0.30 - j1.7	- 0.0074 - j0.31	- j0.0099
λ_3	- 0.036	- 0.038	- 0.0004 + j0.005
λ_4	- 0.59	- 0.40	- 0.0004 - j0.005
λ_5	0	0	0
λ_6	0	0	0
λ_7	0	0	0
λ_8	0	0	0
λ_9	- 0.63	- 0.63	- 0.63
λ_{10}	- 0.63	- 0.63	- 0.63
λ_{11}	- 1000	- 1.0	- 0.001
λ_{12}	- 1000	- 1.0	- 0.001
λ_{13}	- 0.63	- 0.62	- 0.0010
λ_{14}	- 0.63	- 0.26	- 0.0004
λ_{15}	- 1000	- 1.0	- 0.63
λ_{16}	- 1000	- 1.4	- 0.84
λ_{17}	- 1001	- 2.4	- 1.7
λ_{18}	- 1031	- 33	- 32

Considering the variance of the time constant τ, the obtained eigenvalues for some selected values ($\tau = 0.001$, $\tau = 1$, $\tau = 1000$) are given in Table 2. It also takes into account that each value of τ corresponds to a respective value of α_1 and β_1 according to (14) and (15). When $\tau = 1000$, the system has an additional pair of eigenvalues with imaginary part different of zero. It indicates a more oscillatory response if compared with other selected values of τ.

With the employment of multiple units with different output rating, the gains kp_1, kq_1 and α_1 are adjusted in conformity with the rating:

$$kp_{11} \cdot S_1 = kp_{12} \cdot S_2 = \ldots = kp_{1N} \cdot S_N$$

$$kq_{11} \cdot S_1 = kq_{12} \cdot S_2 = \ldots = kq_{1N} \cdot S_N$$

Table 3: Eigenvalues of matrix **A** for selected values of kp_1 and kq_1

	$kp_{11} = kq_{11} = 0.1$ $kp_{12} = kq_{12} = 0.2$	$kp_{11} = kq_{11} = 1$ $kp_{12} = kq_{12} = 2$
λ_1	- 0.014 + j0.64	- 0.0038 + j0.22
λ_2	- 0.014 - j0.64	- 0.0038 - j0.22
λ_3	- 0.037	- 0.038
λ_4	- 0.50	- 0.33
λ_5	0	0
λ_6	0	0
λ_7	0	0
λ_8	0	0
λ_9	- 0.63	- 0.63
λ_{10}	- 0.63	- 0.63
λ_{11}	- 1.0	- 1.0
λ_{12}	- 1.0	- 1.0
λ_{13}	- 0.63	- 0.61
λ_{14}	- 0.46	- 0.18
λ_{15}	- 1.0	- 1.0
λ_{16}	- 1.1	- 1.7
λ_{17}	- 1.4	- 3.5
λ_{18}	- 7.9	- 64

Table 4: Eigenvalues of matrix **A** for selected values of α_1

	$\alpha_{11} = 0.01$ $\alpha_{12} = 0.02$	$\alpha_{11} = 0.1$ $\alpha_{12} = 0.2$
λ_1	- 0.0090 + j0.14	- 0.0060 + j0.44
λ_2	- 0.0090 - j0.14	- 0.0060 - j0.44
λ_3	- 0.0069	- 0.090
λ_4	- 0.44	- 0.33
λ_5	0	0
λ_6	0	0
λ_7	0	0
λ_8	0	0
λ_9	- 0.63	- 0.63
λ_{10}	- 0.63	- 0.63
λ_{11}	- 1.0	- 1.0
λ_{12}	- 1.0	- 1.0
λ_{13}	- 0.62	- 0.62
λ_{14}	- 0.26	- 0.27
λ_{15}	- 1.0	- 1.0
λ_{16}	- 1.4	- 1.4
λ_{17}	- 2.4	- 2.4
λ_{18}	- 33	- 33

$$\alpha_{11} \cdot S_1 = \alpha_{12} \cdot S_2 = \ldots = \alpha_{1N} \cdot S_N$$

where S_n is the output power rating of the unit n ($n = 1, 2, \cdots, N$).

In case of variation of the gains kp_1 and kq_1, the eigenvalues for some points are shown in the Table 3. For $kp_{11} = kq_{11} = 0.5$ and $kp_{12} = kq_{12} = 1.0$, the eigenvalues are the same when $\tau = 1$ in Table 2. Lower values of kp_1 and kq_1 present higher value of the module of the imaginary part in λ_1 and λ_2. Besides that, most of the eigenvalues become closer to the origin as the lower kp_1 and kq_1. Thus, it evidences a less stable response for lower values of kp_1 and kq_1.

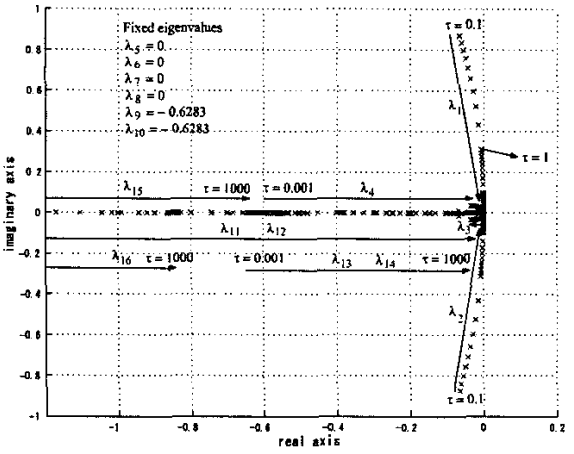

Fig. 3: Detail of the root locus diagram for $0.001 \leq \tau \leq 1000$

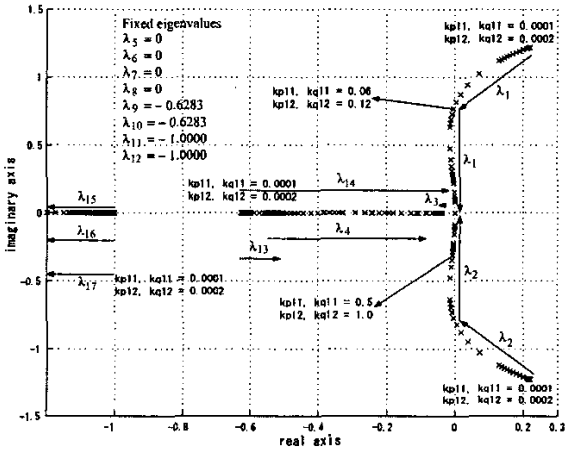

Fig. 4: Detail of the root locus diagram for $0.0001 \leq kp_{11} = kq_{11} \leq 7$ and $0.0002 \leq kp_{12} = kq_{12} \leq 14$

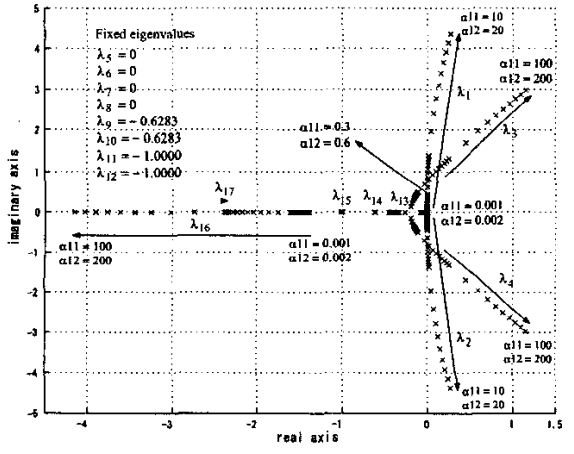

Fig. 5: Detail of the root locus diagram for $0.001 \leq \alpha_{11} \leq 100$ and $0.002 \leq \alpha_{12} \leq 200$

Table 4 presents the obtained eigenvalues for selected values for the gain α_1. For $\alpha_{11} = 0.05$ and $\alpha_{12} = 0.10$, the obtained eigenvalues are equal to the case of $\tau = 1$ in the Table 2. The variation of the module of the obtained eigenvalues with the changing of the gain α_1 is less significant than in other verified situations.

In all the calculations, there are two pairs of eigenvalues which are equal to zero. One pair is associated with the proportional integral characteristic of hs. Another pair is due to $\alpha_2 = 0$.

2.5. *Root Locus Diagram*

The results obtained previously by selecting some values for the gains of the control equations can be extended for an entire range with many points. As a result, root locus diagrams can provide much more information about the performance of the parallel-connected UPS's system.

Fig. 3 shows a detailed part of a root locus diagram when τ varies from 0.001 to 1000. Most of the eigenvalues can be seen in Fig. 3. The arrows roughly indicate the gradient of the corresponding eigenvalue for the interval in consideration. About the eigenvalues which are uncovered in Fig. 3: λ_{11} and λ_{12} vary from -1000 to -0.001; λ_{15} varies from -1000 to -0.63; λ_{16} varies from -1000 to -0.84; and λ_{18} varies from -1031 to -32.

Considering the root locus diagram for the interval $0.0001 \leq kp_{11} = kq_{11} \leq 7$ and $0.0002 \leq kp_{12} = kq_{12} \leq 14$ as seen in Fig. 4, we realize that the system has an unstable region for lower values of kp_1 and kq_1. On the other hand, higher values of kp_1 and kq_1 (> 1) mean high variation of the system variables and the small-signal model may not be valid at all. λ_{16} varies from -1.0 to -4.4; λ_{17} varies from -1.0 to -16; and λ_{18} varies from -2.1 to -439.

The interval $0.001 \leq \alpha_{11} \leq 100$ and $0.002 \leq \alpha_{12} \leq 200$ has an unstable region for higher values of α_{11} and α_{12} as seen in Fig. 5. With lower values of α_{11} and α_{12}, the eigenvalues approaches to zero as shown in Fig. 5 and it can represent a loss of stiffness. λ_{18} varies from -33 to -37.

The waveform response obtained by computer simulations confirms the system unstability when a gain related to the eigenvalues of the unstable region is employed.

3.0. Experiments

3.1. *Description of the Experimental Set*

Some results using two units have been shown in [5] and [8]. The present paper performs the experimental verification of the independent control theory by means of an experimental set with three single-phase UPS's of different output rating (the ratio is 3:2:1) connected in parallel and assembled according to the scheme in the Fig. 6. A power amplifier connected in series with a RL impedance constitutes each UPS. The control software defines each voltage waveform which is directed to its corresponding power amplifier in order to operate the system.

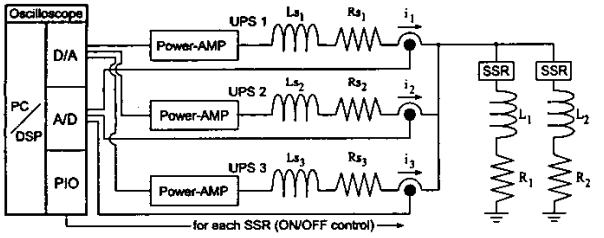

Fig. 6: Scheme for the experiments

The independent control and the switching of the solid state relay - SSR (EZ240D5) - are also functions of the software. With the measurement of the output current, the calculation of the active and reactive components and the control are accomplished by a digital signal processor - DSP (TMS320C32-50MHz). The monitoring of the system and data acquisition are accomplished by operating a 200-Mhz PC computer.

The control equation for hs is taken to be (16). Although (17) was considered in the small-signal analysis, (3) is the control equation for dv in the experiments.

Due to the control software and the system configuration, four kinds of conditions can be verified here: i) without intervention; ii) voltage phase shift in any UPS; iii) change of amplitude of the voltage in any UPS; and iv) change of load by switching the SSR's. The first condition does not exert stress into the system so it is not covered in this paper. By setting the voltage parameters in the control software, it introduces disturbances allowing the verification of the second and third conditions. Also by the control software, the switching of the SSR's allows the changing of the load.

In the following experimental results, the condition with voltage phase shift is performed by shifting, at $t = 30s$, the voltage phase of UPS # 2 ($+2.5\,°$) and UPS # 3 ($-5\,°$). The change of amplitude of the voltage is done, at $t = 30s$, in UPS # 2 ($+0.2$ V) and UPS # 3 (-0.4 V). The verification of change of load follows the schedule shown in Table 5.

Table 5: Load resistance and inductance

Period [s]	R [Ω]	L [mH]	Load status
$0 \sim 40$	50	100	100%
$40 \sim 70$	100	200	50%
$70 \sim 100$	0	0	0%

For all experiments, the voltage V_M is taken to be $80\sqrt{2}$ [V], and the nominal frequency is taken to be 50 [Hz]. Other parameters of the circuit are defined as in Table 6.

3.2. *Variation of τ*

In the previous section, we have seen the prediction of the performance of the system by computation of the eigenvalues of the matrix **A** under the variation of certain gains. In order to confirm the results in terms of the variance of the time constant τ, some experiments using three single-phase parallel-connected UPS's system are performed using the same selected values for τ ($\tau = 0.001$, $\tau = 1$, and $\tau = 1000$). In case of $\tau = 1$, the parameters are given in Table 6. By using (14) and (15), new values of α_1 and β_1 are calculated for $\tau = 0.001$ ($\alpha_{11} = 50$, $\alpha_{12} = 100$, $\alpha_{13} = 150$, $\beta_1 = 1000$) and $\tau = 1000$ ($\alpha_{11} = 0.00005$, $\alpha_{12} = 0.00010$, $\alpha_{13} = 0.00015$, $\beta_1 = 0.001$). Other parameters remain as in Table 6.

Table 6: Parameters used in the experiments

	UPS 1		UPS 2		UPS 3
Rs_1	0.5 Ω	Rs_2	1 Ω	Rs_3	1.5 Ω
Ls_1	1 mH	Ls_2	2 mH	Ls_3	3 mH
I_{pref}	0.28 A	I_{pref}	0.14 A	I_{pref}	0.09 A
I_{qref}	0.15 A	I_{qref}	0.08 A	I_{qref}	0.05 A
β_1	1	β_1	1	β_1	1
α_1	0.05	α_1	0.10	α_1	0.15
kq_2	0	kq_2	0	kq_2	0
a	0.63	a	0.63	a	0.63
kp_1	0.5	kp_1	1.0	kp_1	1.5
kq_1	0.5	kq_1	1.0	kq_1	1.5

Using the parameters given in Table 6 ($\tau = 1$) and shifting the voltage phase, the waveforms of the active and reactive currents are shown in Fig. 7 and Fig. 8, respectively. Changing the value of τ, it results in a different response specially in the time response of the active current waveforms as seen in Fig. 9 for $\tau = 1000$.

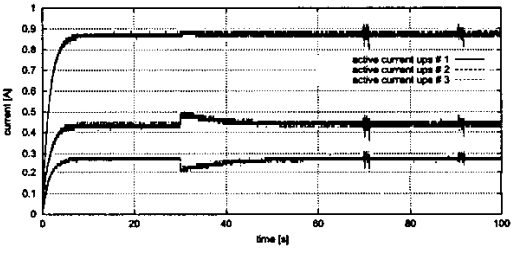

Fig. 7: Active current waveforms when some UPS's suffer a voltage phase shift using the parameters given in Table 6

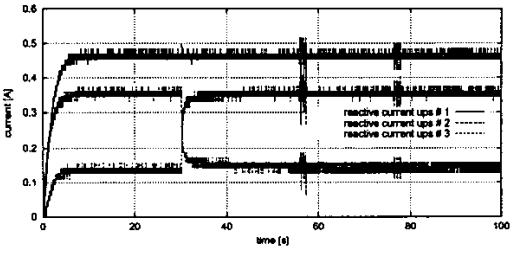

Fig. 8: Reactive current waveforms when some UPS's suffer a voltage phase shift using the parameters given in Table 6

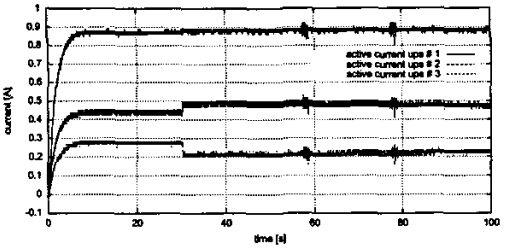

Fig. 9: Active current waveforms for $\tau = 1000$ in case of voltage phase shift

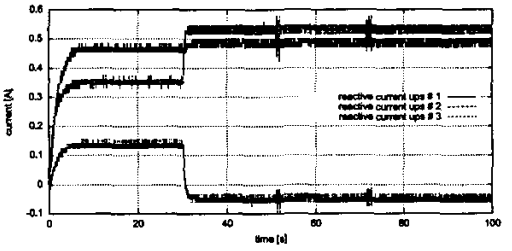

Fig. 10: Reactive current waveforms when some UPS's suffer a change of the amplitude of the voltage using the parameters given in Table 6

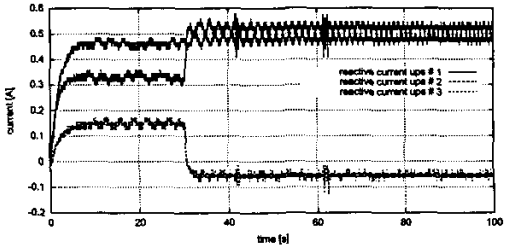

Fig. 11: Reactive current waveforms for $\tau = 1000$ in case of change of the amplitude of the voltage

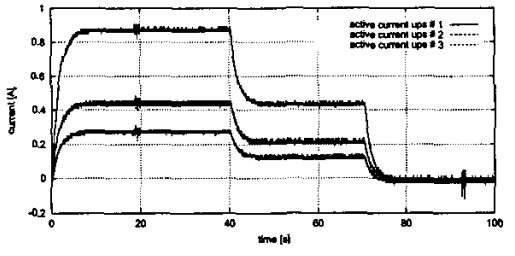

Fig. 12: Active current waveforms for $\tau = 0.001$ when the load changes

When the amplitude of the voltage changes, the active current response is steady, undeformed and practically the same for all values of τ. Fig. 10 shows the response of the reactive current under such disturbance. It evidences the presence of lateral reactive current flow between the UPS's due to the interaction of this type of connection. As the higher τ, the response of the reactive current waveforms is more oscillatory as seen in Fig. 11. It confirms the analysis shown in Section 2.

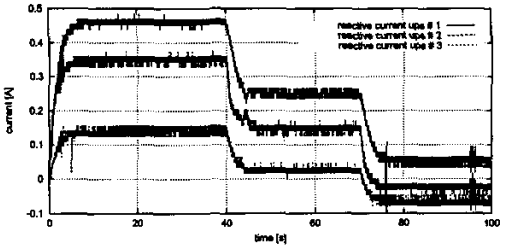

Fig. 13: Reactive current waveforms for $\tau = 0.001$ when the load changes

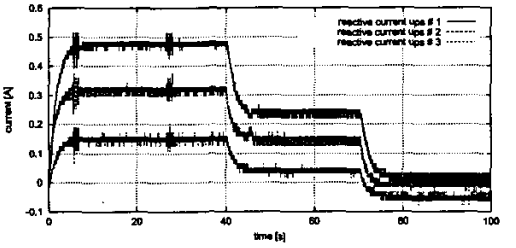

Fig. 14: Reactive current waveforms for higher values of kp_1 and kq_1 in case of change of load

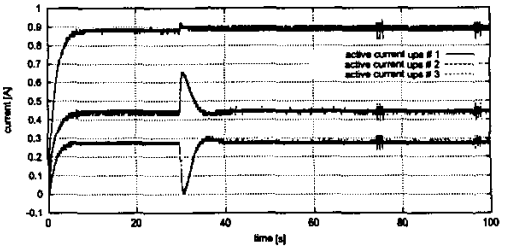

Fig. 15: Active current waveforms for lower values of kp_1 and kq_1 in case of voltage phase shift

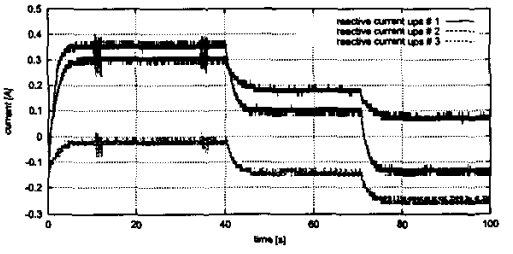

Fig. 16: Reactive current waveforms for lower values of kp_1 and kq_1 in case of change of load

In case of change of load, the active current is well balanced as shown, for example, in the Fig. 12. This characteristic is observed in the entire selected range for τ. The response of the reactive current is affected by the lateral reactive power flow as seen in the Fig. 13. Also here, an oscillation exists in the reactive current waveform when $\tau = 1000$. Such fact is verified in all conditions.

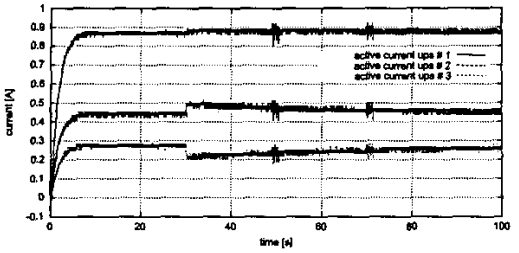

Fig. 17: Active current waveforms for lower values of α_1 in case of voltage phase shift

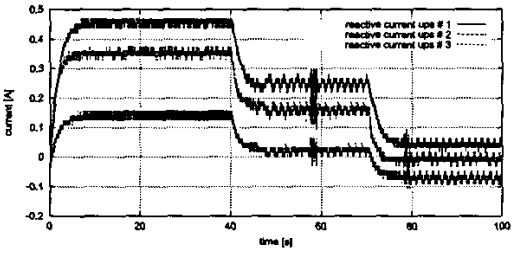

Fig. 18: Reactive current waveforms for lower values of α_1 when the load changes

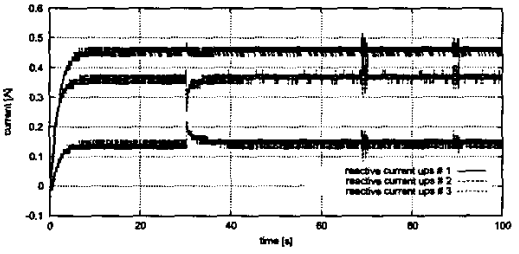

Fig. 19: Reactive current waveforms for higher values of α_1 in case of voltage phase shift

3.3. *Variation of kp_1 and kq_1*

The variation of kp_1 and kq_1 has considerable results in all conditions. Higher values of kp_1 and kq_1 may invalidate the small-signal model. However, for $kp_{11} = kq_{11} = 1$, $kp_{12} = kq_{12} = 2$, and $kp_{13} = kq_{13} = 3$, the experiments show small variation of the active and reactive components in case of voltage phase shift. It also perform a better balance of the reactive current in case of change of load as shown in Fig 14. With lower values of kp_1 and kq_1, the system approaches the unstable region. For $kp_{11} = kq_{11} = 0.1$, $kp_{12} = kq_{12} = 0.2$, and $kp_{12} = kq_{12} = 0.3$), the current components present higher variation under disturbances and a worse balance of reactive current. It is clearly seen in Fig. 15 in case of voltage phase shift and in Fig. 16 in case of change of load.

3.4. *Variation of α_1*

Experimental results using lower values of α_1 (α_{11}) = 0.01, $\alpha_{12} = 0.02$, $\alpha_{13} = 0.03$) show a slower response in case of voltage phase shift (Fig. 17). In addition, it has observed an oscillation in the reactive current in case of change of load as seen in Fig. 18. While in the stable region, higher values of α_1 ($\alpha_{11} = 0.1$, $\alpha_{12} = 0.2$, $\alpha_{13} = 0.3$) imply in a faster response as, for example, in comparison between the response in Fig. 19 and in Fig. 8.

4. Conclusions

This paper has proposed an independent control law in which its feasibility is accomplished by controlling the phase angle and amplitude of the voltage source of the UPS. One explanation of this control technique is derived from the swing equation (synchronous machine model) and a small-signal analysis proves the stability of the parallel-connected multi UPS's system. The calculation of the eigenvalues of the matrix **A** of the system allows the plotting of root locus diagrams which gives a better description of the behavior of the system. In order to confirm the theoretical discussions, experiments using three single-phase parallel-connected multi UPS's system are performed where the synchronization and load sharing are accomplished with excellent performance. These results also suggest that the independent control can be employed successfully in a system with N units where it should be addressed to a future work.

References

[1] T. Kawabata, and S. Higashino, "Parallel operation of voltage source inverters", *IEEE Trans. Ind. Applicat.*, vol. 24, pp. 281-287, Mar./Apr. 1988.

[2] M. C. Chandorkar, D. M. Divan, and B. Banerjee, "Control of distributed ups systems", *Proc. of IEEE PESC94*, pp. 197-204, 1994.

[3] A. Kawamura, and R. Watanabe, "Autonomously decentralized control of multiple ups's for higher reliability", *Proc. of ICPE'98*, pp. 836-840, 1998.

[4] A. Kawamura, and E. K. Sato, "One explanation of the independent control law for parallel-connected ups", *Proc. of IEE Japan Industry Appl. Soc. Conf.*, No. 83, pp. 389-390, 2002.

[5] E. K. Sato, and A. Kawamura, "Analysis and experiments on independent control for parallel-connected ups based on swing equation", *Proc. of IEE Japan Industry Appl. Soc. Conf.*, 2003 (to be published)

[6] E. A. A. Coelho, P. C. Cortizo, and P. F. D. Garcia, "Small-signal stability for parallel-connected inverters in stand-alone ac supply systems", *IEEE Trans. Ind. Applicat.*, vol. 38, pp. 533-542, Mar./Apr. 2002.

[7] E. K. Sato, and A. Kawamura, "Linearized expression of active and reactive current in parallel-connected ups system", *Proc. of IEE Japan National Convention*, No. 4-113, pp. 173-174, 2003.

[8] A. Kawamura, and R. Fujii, "Experiments for independent control of ups based on complex systems", *Proc. of IEE Japan Industry Appl. Soc. Conf.*, No.250, pp. 1311-1314 (2002) (in Japanese)